P1.1 TWO CONTRASTING CASE STUDIES OF ENTRAINMENT ZONE STRUCTURE IN CLOUD CAPPED MARINE ATMOSPHERIC BOUNDARY LAYERS

Ian M. Brooks*
University of Leeds, Leeds, UK

1. INTRODUCTION

Entrainment is an important factor in controlling both the distribution and structure of stratocumulus, both though its contribution to the rate of change of boundary-layer (BL) depth, and by directly modifying the microphysical properties of the cloud as warm dry air is mixed with cloudy air. The large spatial extent of marine stratocumulus makes it, and thus entrainment, an important factor in the global radiation budget. In spite of its importance entrainment remains poorly understood and poorly represented within climate models.

Direct measurement of the entrainment rate is not possible, and it must be inferred from other measurements (Lenschow et al. 1999). In contrast, the structure of the entrainment zone is relatively easy to characterize using instruments such as lidar, and is usually assumed to be directly related to the entrainment rate. Studying the structure of the entrainment zone provides a means of trying to understand the nature of the entrainment process.

2. MEASUREMENTS

The measurements presented here are drawn from two flights off the coast of northern California made by the NCAR C-130 Hercules during the Coastal Waves '96 field program in June 1996. The flights were made on June 12 around Cape Medocino and June 21 around Point Sur (Fig. 1).

Lidar measurements of cloud top height were obtained with the NCAR Scanning/Staring Aerosol Backscatter Lidar (SABL) during flight legs above the boundary layer. SABL operates at two wavelengths: 532 and 1064 nm; only the 1064 nm data has been used in this analysis, primarily because the 532 nm data suffered from a larger '*dead zone*' – the region close to the aircraft where the signal is saturated – which encompassed cloud top during parts of the flight legs, making this data unusable. During this study SABL was operated with a range resolution of 3.75 m; backscatter profiles were obtained at a rate of 20 Hz, providing a horizontal resolution of approximately 5 m at the aircraft's nominal science speed of 100 m s^{-1}.

Cloud top was identified from the backscatter signal by means of a wavelet covariance transform – steps in the backscatter signal are identified by local maxima in the covariance between the signal and a Haar function (Davis et al. 2000). The timeseries of cloud-top

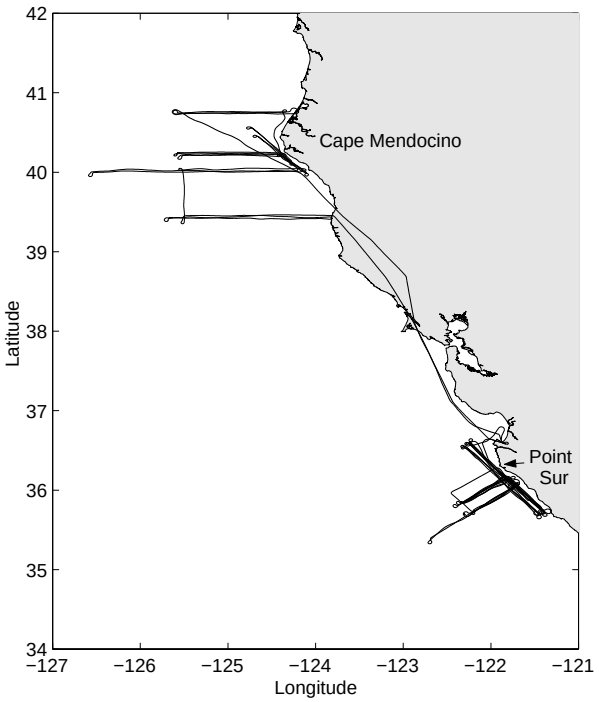

Figure 1. Flight tracks for June 12, around Cape Mendocino, and Jun 21, around Point Sur.

estimates was then filtered with a 3-point median filter to remove outliers; points differing from the filtered values by more than 3 range gates were replaced by the filtered values; less than 0.5% of cloud-top estimates required correction in this manner. Entrainment is an inherently small-scale turbulent process; variations in cloud top on scales greater than that of the largest turbulent motions are due to gravity waves and mesoscale variability in BL depth, and should not be included in the assessment of entrainment zone structure. Thus, before calculating entrainment zone statistics, the cloud-top heights are high-pass filtered to remove wavelengths greater than ~1 km, the upper limit of observed turbulence within these boundary layers.

Measurements of boundary-layer structure were made by a series of sawtooth profiles from 15 m to just above BL top along the same ground-track as the high level flight legs. Although the only straight and level flight legs suitable for deriving robust turbulence measurements were made at 30 m altitude, the general turbulence structure of the boundary layer can be derived from the profiles as described in Brooks et al. (2003). The high-rate (25-Hz) data were high-pass filtered to remove the slowly varying mean, and series of

* *Corresponding Author address*: Ian M. Brooks, Institute for Atmospheric Science, School of the Environment, University of Leeds, Leeds, LS2 9JT, UK; e-mail: ibrooks@env.leeds.ac.uk

instantaneous second-order moments obtained as the product of two filtered time-series. Local values of the turbulence quantities were then obtained by block-averaging over an interval sufficient to encompass all the scales contributing significantly to the second-order moments. Here a horizontal distance of 1-km was found to be just sufficient; this corresponds to approximately 50 m in the vertical.

3. RESULTS

Entrainment-zone depth was defined as the vertical interval over which between 5% and 95% of the air originates from above the BL, as determined from the probability distribution of cloud-top heights and following many previous studies (e.g. Deardorff et al. 1980, Melfi et al. 1985, Nelson et al. 1989). Prior to calculating the entrainment zone depth, the observations were split into subsets for which both the mean BL depth and degree of cloud-top variability were relatively uniform; to provide individual estimates for regions with different mean properties. Associated with each are one or more vertical profiles.

Figure 2 shows the entrainment zone depths plotted against a bulk Richardson number, Ri_b, calculated across the inversion layer. Ri_b spans a similar range of values on both days, however the entrainment zone depths behave very differently. On June 12 there is a clear inverse relationship between the entrainment zone depth and Ri_b; this is expected since the entrainment rate is known to be related to the inverse of the Richardson number (Moeng et al. 1999). On June 21 there is no variation in the entrainment zone depth at all, and it is approximately equal to the minimum observed on June 12. The difference in behavior between these two cases can be explained by a close examination of the vertical profiles through the BL and cloud top. Figures 3 and 4 show representative profiles of virtual potential temperature, liquid water content, mean wind speed, the gradient Richardson number, the vertical velocity variance, and buoyancy flux for June 12 and June 21 respectively. On both days

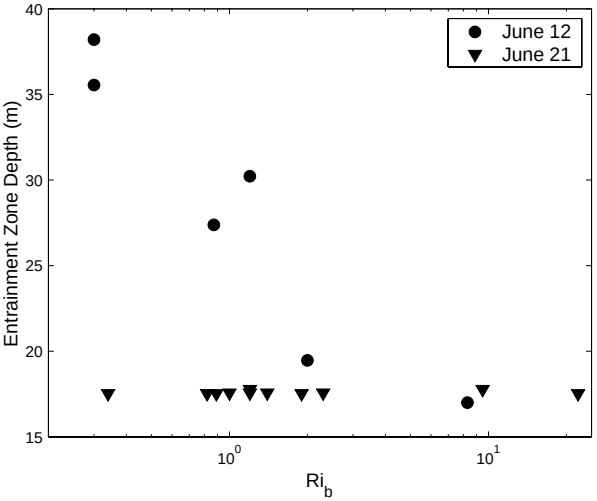

Figure 2. Entrainment zone depth plotted against the bulk Richardson number.

the upper boundary layer and cloud deck are decoupled from the surface by a stable internal boundary layer (IBL). This is clearly seen in the profiles of mean wind, where shear is largely confined to the internal boundary layer and the speed is near-constant throughout the upper BL; in the vertical velocity variance, which shows a distinct minimum in turbulence intensity just above the IBL, and in the buoyancy flux which is negative at the surface and falls to zero at the top of the IBL. The decoupling is strongest on June 21, as indicated by the fall of the vertical velocity variance to almost zero between about 200 and 400 m; turbulence is generally weaker throughout the BL on June 21. The turbulence intensity increases again higher in the BL and shows local maxima within the cloud layer on both days. The buoyancy flux is positive within the cloud layer on both days, indicating that turbulence is being generated by buoyant convection. This must be driven primarily by radiative forcing, but there may also be a contribution from buoyancy reversal following the mixing of clear and cloudy air (see below). Wind shear across the inversion

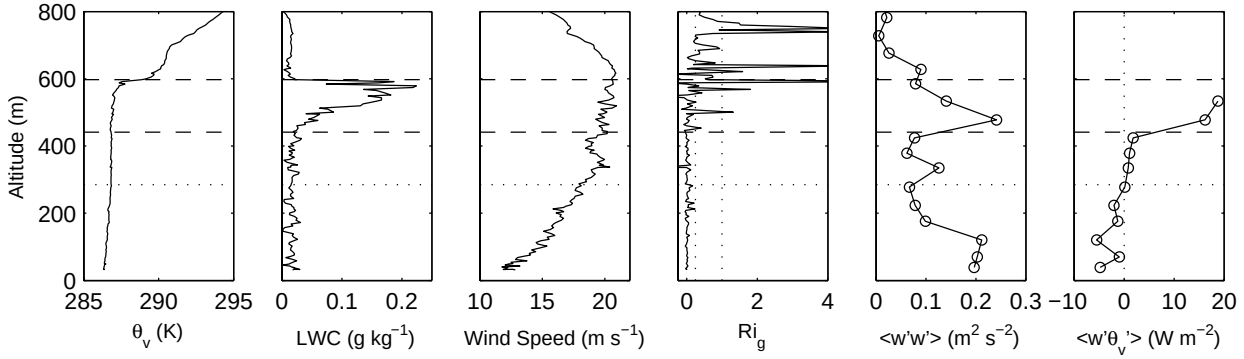

Figure 3.. Profiles of virtual potential temperature, liquid water content, wind speed, gradient Richardson number, vertical velocity variance, and buoyancy flux. Cloud base and top are indicated by dashed lines and the top of the internal boundary layer by a horizontal dotted line; vertical dotted lines indicate Richardson numbers of 0.25 and 1. Profile made at 17:59 UTC on June 12.

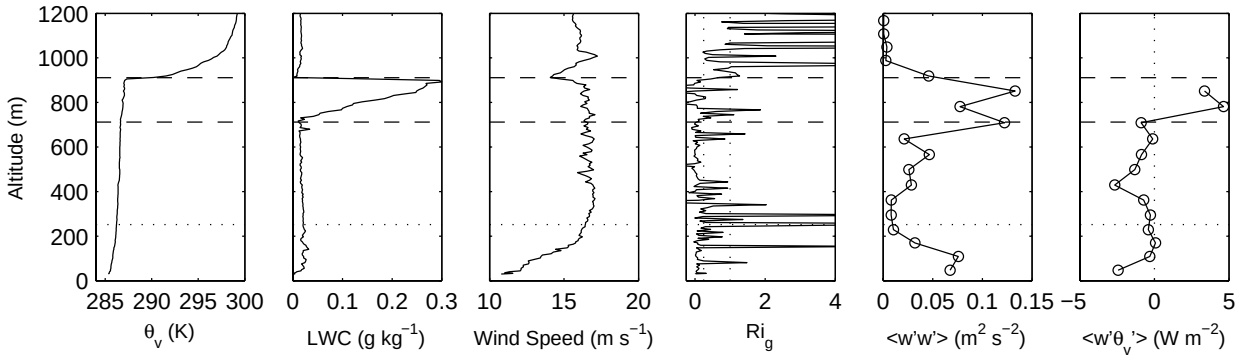

Figure 4.. As figure 3 but for 23:21 UTC on June 21.

might also contribute to turbulence generation. The general structure described above is very similar for both cases, but there are significant differences just above cloud top. On June 12 there is a layer approximately 100 m deep in which turbulence is maintained above the cloud. This is clearly seen in the profile of vertical velocity variance. The inversion at cloud top is sharp, but relatively weak – about 2.5 K, strong stable stratification continues above the 100-m turbulent layer. On June 21 turbulence drops to zero immediately above cloud top. The inversion is rather stronger – a sharp jump of 2-3 K immediately above cloud, and then a continuous layer of slowly weakening stable stratification above that; the total increase in θ_v is over 10 K. The turbulence structure through cloud top is reflected in the profiles of gradient Richardson number Ri_g, which remains < 1, except for two narrow spike, up to 100 m above cloud top on June 12, but increases above 1 at cloud top on June 21.

The strong inversion on June 21 appears to suppress any variability in the entrainment zone depth, while the existence of a 100-m deep layer in which turbulence can be supported above a weak inversion at cloud top on June 12 means allows the entrainment zone to respond to small changes in the conditions at cloud top.

It was noted above that buoyancy reversal following the mixing of clear and cloudy air might contribute to the generation of turbulence in cloud. The condition for a mixture of entrained and cloudy air to be negatively buoyant with respect to unmixed cloudy air is

$$R \equiv \frac{c_p \Delta\theta_e}{L_v \Delta Q_t} > 0.23 \qquad (1)$$

(Lock and MacVean 1999) where c_p is the specific heat of air at constant pressure, L_v is the latent heat of vaporization of water, θ_e is the equivalent potential temperature, and Q_t is the total water mixing ratio. R was evaluated for each profile through cloud top: on June 12 the values ranged from -1.1 to 0.3 with a mean of -0.23, and a standard deviation of 0.45; on June 21 they ranged from -0.5 to 3.5 with a mean of 0.86, and a standard deviation of 0.9. The buoyancy reversal condition is thus satisfied on June 21 but not on June 12.

Figure 5. shows the entrainment zone depths plotted against cloud depth. Both days display a similar range of cloud depths. There is, of course, no variability on June 21, but on June 12 there is a clear inverse relationship.

4. SUMMARY AND CONCLUSIONS

High resolution lidar measurements of cloud top height have been used to evaluate a measure of entrainment-zone depth for two stratocumulus topped boundary layers. In both cases the boundary layers are decouple from the surface by a stable internal boundary layer, so that entrainment must be driven by turbulence generated in cloud. The two cases display rather different behavior: in one (June 12) there is a clear inverse relationship between the entrainment zone depth and the Richardson number calculated across the inversion; the other case (June 21) displays no variability at all; the range of Richardson numbers is

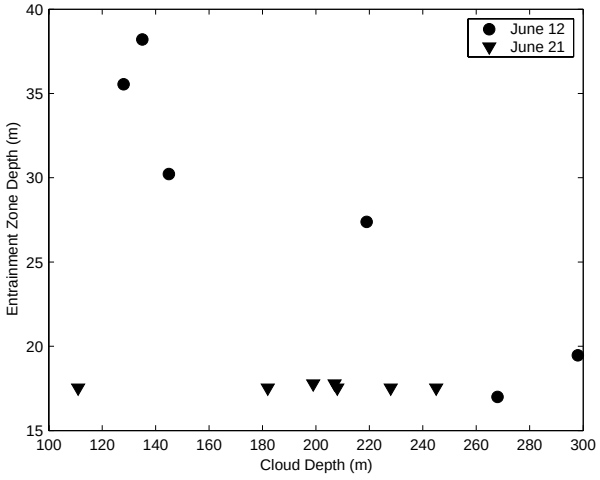

Figure 5. Entrainment zone depth plotted against the local cloud depth.

similar in both cases. The difference in behavior appears to be due to differences in the stratification just above cloud top. On June 21 there is a strong, continuous inversion layer. Given the extreme uniformity in the observed entrainment zone depth, it is suggested that entrainment may be completely inhibited in this case, and that the variation in cloud-top height from which entrainment zone depth is determined is merely due to local perturbations of the inversion and not mixing of air down into the cloud. It is notable that the calculated entrainment zone depth in this case is equal to the minimum observed on June 12. On June 12 a layer 100 m deep exists above cloud top in which turbulence can be maintained. Turbulence is thus continuous, if weak, across cloud top, and the entrainment process, and hence entrainment zone depth, responds readily to small changes in the conditions at cloud top.

The buoyancy reversal criterion suggests that this process does not contribute to turbulence generation on June 12, but is satisfied on June 21 so that it could contribute if any mixing were to take place.

On June 12 there is an inverse relationship between the depths of the entrainment zone and the cloud layer.

5. REFERENCES

Brooks, I. M., S. Söderberg, and M. Tjernström, 2003: The turbulence structure of the stable atmospheric boundary layer around a coastal headland: aircraft observations and modelling results. *Bound.-Layer Meteorol.*, **107**, 531-559.

Davis, K. J., N. Gamage, C. R. Hagelberg, C. Kiemle, D. H. Lenschow, and P. P. Sullivan, 2000: An objective method for deriving atmospheric structure from airborne lidar observations. *J. Atmos. Oceanic. Technol.*, **17**, 1455-1468.

Deardorff, J. W., G. E. Willis, and B. H. Stockton, 1980: Laboratory studies of the entrainment zone of a convectively mixed layer. *J. Fluid Mech.*, **100**, 41-64.

Lenschow, D. H., P. B. Krummel, and S. T. Siems, 1999: Measuring entrainment, divergence, and vorticity on the mesoscale from aircraft. *J. Atmos. Oceanic. Tech.*, **16**, 1384-1400.

Lock, A. P., and M. K. MacVean, 1999: The generation of turbulence and entrainment by buoyancy reversal. *Quart. J. Royal Meteorol. Soc.*, **125**, 1017-1038.

Melfi, S. H., J. D. Sphinhirne, S. H. Chou, and S. P. Palm, 1985: Lidar observations of the vertically organized convection in the planetary boundary layer over the ocean. *J. climate Appl. Meteorol.*, **24**, 806-821.

Moeng, C.-H., P. P. Sullivan, and B. Stevens, 1999: Including radiative effects in an entrainment rate formula for buoyancy-driven PBLs. *J. Atmos. Sci.*, **56**, 1031-1049.

Nelson, E., R. B. Stull, and E. Eloranta, 1989: A prognostic relationship for entrainment zone thickness. *J. Applied Meteorol.*, **28**, 885-903.